Nanosized SAPO-34 Synthesized from Colloidal Solutions

Hendrik van Heyden,[†] Svetlana Mintova,*[,‡] and Thomas Bein*[,†]

Department Chemistry & Biochemistry, University of Munich, Germany, and Laboratoire de Matériaux à Porosité controlée, UMR 7016 CNRS, Mulhouse, France

Received December 12, 2007. Revised Manuscript Received January 27, 2008

Nanosized SAPO-34 (100–500 nm) was synthesized from colloidal solutions in the presence of tetraethylammonium hydroxide as a template at different hydrothermal (HT) conditions carried out in conventional and microwave ovens. The smallest SAPO-34 particles (~100 nm) were obtained from the colloidal solutions with a molar composition of 1 Al_2O_3:2 P_2O_5:0.6 SiO_2:2 TEA_2O:75 H_2O using microwave energy. The stability and degree of polydispersity of the nanosized crystalline SAPO-34 product were determined by dynamic light scattering and zeta potential measurements in aqueous suspensions. The isoelectric point for the SAPO-34 particles is at pH ~ 4 due to its acidity, which is dependent on the degree and distribution of silicon in the CHA-type framework. The effect of crystal size on the sorption properties of SAPO-34 crystals was studied by Argon physisorption at 87 K, where a high degree of textural porosity responsible for a large fraction of the total volume adsorbed is measured.

Introduction

The reduction of zeolite crystal size has been a major research field for the past 10 years as the decrease of dimension leads to substantial changes in the properties of the materials.[1] Primarily, this has an impact on the performance of zeolites in traditional application areas such as catalysis and separation.[2–4] Additionally, this development has led to developments of new synthesis strategies yielding nanomaterials with narrow particle size distributions. Moreover, the possibility of stabilizing these nanoparticles in suspensions has facilitated the production of thin-to-thick films, which are interesting for membrane and sensing applications.[5–12] The most promising route for preparation of microporous and particularly zeolite nanocrystals is the use of clear solutions or colloidal suspensions as precursor media. An excellent review summarizing all the studied systems was published from Tosheva and Valtchev.[1] This article mainly deals with zeolite syntheses, but also aluminophosphate systems are discussed, namely, $AlPO_n$-5 (AFI), $AlPO_n$-11 (AEL), and $AlPO_n$-18 (AEI). The $AlPO_n$-18 system is the most investigated colloidal aluminophosphate because of the superior water sorption properties.[13] A structurally related system is $AlPO_n$-34 with chabazite structure (CHA); the silicon-substituted form $SAPO_n$-34 is one of the widely investigated molecular sieves due to the use in catalysis, especially in the methanol-to-olefin (MTO) process.[14] Besides, SAPO-34 shows unique water sorption properties, which can be used for the thermochemical storage of heat.[15–17] From approximately 600 publications concerning the SAPO-34 material only a few shall be mentioned here. Originally discovered at Union Carbide Corporation,[18,19] the crystal structure of SAPO-34 and its analogy to natural chabazite was first reported by Ito et al.[20] (the analogy to the CHA structure was already reported with the discovery). Numerous groups have investigated the SAPO-34 material in respect to further applications and mainly the performance in the MTO reaction.[21] Apart from its unique pore structure, the short- and long-term hydrothermal stability which is dependent on the degree and homogeneity of the silicon incorporated in the CHA framework is of significant

* Corresponding author. Tel.: (33) 03 89 33 67 39. Fax: (33) 03 89 33 68 85.
† University of Munich.
‡ UMR 7016 CNRS.

(1) Tosheva, L.; Valtchev, V. P. *Chem. Mater.* **2005**, *17*, 2494.
(2) Botella, P.; Corma, A.; Iborra, S.; Monton, R.; Rodriguez, I.; Costa, V. *J. Catal.* **2007**, *250*, 161.
(3) Waller, P.; Shan, Z.; Marchese, L.; Tartaglione, G.; Zhou, W.; Jansen, J. C.; Maschmeyer, T. *Chem.—Eur. J.* **2004**, *10*, 4970.
(4) Grassian, V. H.; Larsen, S. C.; Alwy, H.; Li, G. *Abstracts of Papers; 225th ACS National Meeting*, New Orleans, March 23−27, 2003; American Chemical Society: Washington, DC, 2003.
(5) Mintova, S.; Bein, T. *Adv. Mater. (Weinheim, Ger.)* **2001**, *13*, 1880.
(6) Mintova, S.; Reinelt, M.; Metzger, T. H.; Senker, J.; Bein, T. *Chem. Commun.* **2003**, 326.
(7) Schoeman, B. J.; Babouchkina, E.; Mintova, S.; Valtchev, V. P.; Sterte, J. *J. Porous. Mater.* **2001**, *8*, 13.
(8) Valtchev, V.; Mintova, S. *Microporous Mesoporous Mater.* **2001**, *43*, 41.
(9) Vilaseca, M.; Mintova, S.; Karaghiosoff, K.; Metzger, T. H.; Bein, T. *Appl. Surf. Sci.* **2004**, *226*, 1.
(10) Vilaseca, M.; Mintova, S.; Valtchev, V.; Metzger, T. H.; Bein, T. *J. Mater. Chem.* **2003**, *13*, 1526.
(11) Zhang, Y.; Chen, F.; Shan, W.; Zhuang, J.; Dong, A.; Cai, W.; Tang, Y. *Microporous Mesoporous Mater.* **2003**, *65*, 277.
(12) Zhou, X.; Yu, T.; Zhang, Y.; Kong, J.; Tang, Y.; Marty, J.-L.; Liu, B. *Electrochem. Commun.* **2007**, *9*, 1525.
(13) van Heyden, H.; Mintova, S.; Bein, T. *J. Mater. Chem.* **2006**, *16*, 514.
(14) Chen, J. Q.; Bozzano, A.; Glover, B.; Fuglerud, T.; Kvisle, S. *Catal. Today* **2005**, *106*, 103.
(15) Jaenchen, J.; Ackermann, D.; Weiler, E.; Stach, H.; Broesicke, W. *Thermochim. Acta* **2005**, *434*, 37.
(16) Kakiuchi, H.; Shimooka, S.; Iwade, M.; Oshima, K.; Yamazak, M.; Terada, S.; Watanabe, H.; Takewaki, T. *Kagaku Kogaku Ronbunshu* **2005**, *31*, 273.
(17) Oshima, K.; Yamazaki, M.; Takewaki, T.; Kakiuchi, H.; Kodama, A. *Kagaku Kogaku Ronbunshu* **2006**, *32*, 518.
(18) Lok, B. M.; Messina, C. A.; Patton, R. L.; Gajek, T. R.; Cannan, T. R.; Flanigen, E. M. Crystalline silicoaluminophosphates. U.S. Patent 4,440,871, 1984.
(19) Lok, B. M.; Messina, C. A.; Patton, R. L.; Gajek, R. T.; Cannan, T. R.; Flanigen, E. M. *J. Am. Chem. Soc.* **1984**, *106*, 6092.
(20) Ito, M.; Shimoyama, Y.; Saito, Y.; Tsurita, Y.; Otake, M. *Acta Crystallogr., Sect. C: Cryst. Struct. Commun.* **1985**, *C41*, 1698.
(21) Wilson, S.; Barger, P. *Microporous Mesoporous Mater.* **1999**, *29*, 117.

10.1021/cm703541w CCC: $40.75
Published on Web 04/09/2008

importance.[22–24] The samples with relatively low amounts of silicon show high stabilities. It was found that the silicon distribution is dependent on the choice of template used during the synthesis, and the most stable samples are obtained from tetraethylammonium-containing precursor suspensions.[25] The mechanism of SAPO-34 crystallization using morpholine as the structure-directing agent was studied in detailed by Vistad et al.[26–28]

Other factors are the acid-site strength[29] and the influence of incorporated transition metals on the stability and performance of SAPO-34 material.[30] The effect of crystal size for the MTO process was investigated, too.[31–34] They separated fractions of different crystal sizes by centrifugation and found the best performance for crystals of sizes smaller than 500 nm. Below this diameter no diffusion limitations are observed during the catalytic reaction. A synthesis route to SAPO-34 crystals with diameters lower than 500 nm with the tetraethylammonium ion as templating agent therefore seems very desirable. Lesch and Patton synthesized SAPO-34 from very diluted solutions but did not include any data concerning particles size.[35] Additionally, Mertens and Strohmaier claimed the reduction of particle size by either using tetraalkyl orthosilicate as the silicon source[36] or dissolving the silicon in organic bases prior to mixing with other reagents.[37] Here, particles of sizes < 100 nm are claimed on the basis of the data accumulated from SEM and broadening of the X-ray diffraction lines. Yao et al. made an attempt to synthesize SAPO-34 in confined polymer spaces.[38] However, the products contained large amounts of micrometer-sized crystals and their reduced crystallinity led to reduced surface areas.

Here, we report the synthesis of nanosized SAPO-34 crystals with narrow particle size distributions by using colloidal precursor solutions. The influence of the initial composition, temperature, and source of heating on crystal dimensions was studied.

Experimental Section

Clear precursor solutions were prepared with the following molar compositions: 1 Al_2O_3:2–4 P_2O_5:0.6–1 SiO_2:2–4 TEA_2O:75–147 H_2O. The synthesis conditions and the resultant phases from different batches are summarized in Table 1. Aluminum isopropoxide (e.g., sample 160/180_4:6.00 g, 29 mmol, Aldrich), colloidal silica (1.72 g, 9 mmol, Ludox HS-30, 30 wt %, Aldrich), and tetraethylammonium hydroxide solution (48.45 g, 115 mmol, 35 wt %, Aldrich) were mixed at room temperature and stirred at 450 rpm for at least 2 h in 180 mL PP-bottles. To the resultant solution, phosphoric acid (13.28 g, 115 mmol, 85 wt %, Aldrich) was added dropwise over a period of 60–150 min to avoid the formation of dense gel particles. It is important to note that the latest step is crucial for the overall process (special care is needed for the solution with the ratio of Al_2O_3:$TEA_2O = 1$: 2, where after the complete dissolution of the Al/Si sources, the acid is added very slowly). If the obtained mixtures were not clear, then white suspensions were formed. At low concentrations of Al_2O_3:$TEA_2O = 1$:4, the obtained precursor solutions did not show a Tyndall effect. The mixture was stirred another 30 min prior to HT treatment. Ten grams of the solution were filled into a 23 mL Teflon-lined stainless steel autoclave (Parr Instrument Company) and heated in a conventional oven. To study the kinetics of crystal growth of SAPO-34, simultaneously 5 autoclaves were used for each precursor solution, and they were quenched after varying synthesis times. Additionally, microwave syntheses were performed using 100 mL autoclaves (Synthos 3000, Anton Paar GmbH). After the synthesis, the suspensions containing nanosized crystals were purified in a series of three steps consisting of high-speed centrifugation (43 000 rcf, 20 min), removal of the supernatant, and redispersion in aqueous KOH solution (pH = 8) using an ultrasonic (US) bath. If no material was separated by centrifugation, then aqueous NaCl solution (15 mM) was used to provoke coagulation prior to the centrifugation. The samples were freeze-dried to avoid agglomeration for further characterization.

Characterization. All samples were investigated by means of dynamic light scattering (DLS) in a Zetasizer Nano-ZS (Malvern Instruments) directly after HT treatment and after the subsequent washing cycles. Zeta potential measurements giving information about the stability of the suspensions were performed using the same instrument. Prior to these analyses, one drop of the final suspensions was added to 1 mL of buffer solution (Hydrion, Aldrich, pH = 2–11), equilibrated for 30 min, and checked for pH using a gel electrode (Mettler Toledo). Powder X-ray diffraction (XRD) patterns of the freeze-dried samples were recorded using a Stoe STADI-P diffractometer (transmission mode, Cu Kα radiation). The product elemental composition was determined by atomic adsorption spectroscopy with a Varian Vista RL CCD instrument. To investigate the size and morphology of the products, scanning electron microscopy (SEM) images were recorded using a JEOL JSM-6500F microscope. Diffuse reflectance infrared Fourier (Bruker Equinox 55) and Raman (Horiba Jobin Yvon LabRAM-HR, Bruker Equinox 55 & FRA Raman module 106 /S) spectroscopy was used to investigate the short-range order within the materials during the crystallization process. Thermogravimetrical analyses (TGA) and differential scanning calorimetry (DSC) were performed on the as-synthesized samples using a Netzsch STA 440 C Jupiter thermobalance. The samples (10 mg) were heated in a stream of synthetic air (50 mL min^{-1}) with a heating rate of 10 K min^{-1} in an alumina crucible in the temperature range 25–900 °C. Selected samples were investigated by means of volumetric argon physisorption experi-

(22) Ashtekar, S.; Chilukuri, S. V. V.; Chakrabarty, D. K. *J. Phys. Chem.* **1994**, *98*, 4878.
(23) Mees, F. D. P.; Martens, L. R. M.; Janssen, M. J. G.; Verberckmoes, A. A.; Vansant, E. F. *Chem. Commun.* **2003**, 44.
(24) Tan, J.; Liu, Z.; Bao, X.; Liu, X.; Han, X.; He, C.; Zhai, R. *Microporous Mesoporous Mater.* **2002**, *53*, 97.
(25) Briend, M.; Vomscheid, R.; Peltre, M. J.; Man, P. P.; Barthomeuf, D. *J. Phys. Chem.* **1995**, *99*, 8270.
(26) Vistad, B.; Akporiaye, D. E.; Lillerud, K. P. *J. Phys. Chem. B* **2001**, *105*, 12437.
(27) Vistad, O. B.; Akporiaye, D. E.; Taulelle, F.; Lillerud, K. P. *Chem. Mater.* **2003**, *15*, 1639.
(28) Vistad, O. B.; Akporiaye, D. E.; Taulelle, F.; Lillerud, K. P. *Chem. Mater.* **2003**, *15*, 1650.
(29) Regli, L.; Bordiga, S.; Lamberti, C.; Lillerud, K. P.; Zones, S. I.; Zecchina, A. *J. Phys. Chem. C* **2007**, *111*, 2992.
(30) Dubois, D. R.; Obrzut, D. L.; Liu, J.; Thundimadathil, J.; Adekkanattu, P. M.; Guin, J. A.; Punnoose, A.; Seehra, M. S. *Fuel Process. Technol.* **2003**, *83*, 203.
(31) Chen, D.; Moljord, K.; Fuglerud, T.; Holmen, A. *Microporous Mesoporous Mater.* **1999**, *29*, 191.
(32) Chen, D.; Rebo, H. P.; Holmen, A. *Chem. Eng. Sci.* **1999**, *54*, 3465.
(33) Chen, D.; Rebo, H. P.; Moljord, K.; Holmen, A. *Ind. Eng. Chem. Res.* **1999**, *38*, 4241.
(34) Dahl, I. M.; Wendelbo, R.; Andersen, A.; Akporiaye, D.; Mostad, H.; Fuglerud, T. *Microporous Mesoporous Mater.* **1999**, *29*, 159.
(35) Lesch, D. A.; Patton, R. L. Solution synthesis of aluminophosphate crystalline compositions. European Patent 293919 A2, 1988.
(36) Mertens, M.; Strohmaier, K. G. Process for manufacturing a silicoaluminophosphate molecular sieve. U.S. Patent 6696032 B2, 2004.
(37) Mertens, M.; Strohmaier, K. G. Process for manufacture of molecular sieves. U.S. Patent 6773688 B2, 2004.
(38) Yao, J.; Wang, H.; Ringer, S. P.; Chan, K.-Y.; Zhang, L.; Xu, N. *Microporous Mesoporous Mater.* **2005**, *85*, 267.

Table 1. Synthesis Conditions and Resulting Products

sample name	precursor comp. (Al_2O_3:P_2O_5:SiO_2:TEA_2O:H_2O)	T (°C)	t (h)	structure type code	particle diameter[a] (nm)	product comp. Al	P	Si	P+Si
160_2_1	1:2:0.6:2:75	160	0.50	amorphous					
160_2_2	1:2:0.6:2:75	160	1.00	amorphous					
160_2_3	1:2:0.6:2:75	160	1.50	AEI	230	0.51	0.45	0.04	0.49
160_2_4	1:2:0.6:2:75	160	2.00	AEI	240	0.51	0.47	0.02	0.49
160_3_1	1:3:0.6:3:111	160	1.30	amorphous					
160_3_2	1:3:0.6:3:111	160	2.50	amorphous					
160_3_3	1:3:0.6:3:111	160	3.50	amorphous					
160_3_4	1:3:0.6:3:111	160	5.75	CHA (AEI)	320	0.50	0.45	0.05	0.50
160_3_5	1:3:0.6:3:111	160	20.00	CHA	356	0.49	0.43	0.08	0.51
160_4_1	1:4:0.6:4:147	160	2.50	amorphous					
160_4_2	1:4:0.6:4:147	160	3.50	AEI	299	0.50	0.47	0.03	0.50
160_4_3	1:4:0.6:4:147	160	5.00	AEI	329	0.51	0.46	0.03	0.49
160_4_4	1:4:0.6:4:147	160	13.50	AEI	340	0.50	0.46	0.04	0.50
160_4_5	1:4:0.6:4:147	160	15.00	CHA	417	0.50	0.42	0.08	0.50
180_2/1_1	1:2:1:2:77	180	0.50	amorphous					
180_2/1_2	1:2:1:2:77	180	1.00	amorphous					
180_2/1_3	1:2:1:2:77	180	1.50	CHA (low yield)	181				
180_2/1_4	1:2:1:2:77	180	2.00	CHA	285	0.51	0.43	0.06	0.49
180_2/1_5	1:2:1:2:77	180	2.50	CHA	272	0.51	0.42	0.07	0.49
180_2_1	1:2:0.6:2:75	180	0.50	amorphous					
180_2_2	1:2:0.6:2:75	180	1.00	amorphous					
180_2_3	1:2:0.6:2:75	180	2.00	CHA	286	0.51	0.42	0.07	0.49
180_2_4	1:2:0.6:2:75	180	4.25	CHA	316	0.52	0.42	0.06	0.48
180_3_1	1:3:0.6:3:111	180	2.00	amorphous					
180_3_2	1:3:0.6:3:111	180	3.00	CHA	264	0.50	0.47	0.03	0.50
180_3_3	1:3:0.6:3:111	180	4.00	CHA	265	0.50	0.46	0.04	0.50
180_3_4	1:3:0.6:3:111	180	6.00	CHA	276	0.49	0.45	0.05	0.51
180_3_5	1:3:0.6:3:111	180	18.50	CHA	507	0.49	0.44	0.08	0.51
180_4_1	1:4:0.6:4:147	180	2.00	amorphous					
180_4_2	1:4:0.6:4:147	180	3.00	amorphous					
180_4_3	1:4:0.6:4:147	180	4.50	CHA	308	0.51	0.46	0.03	0.49
180_4_4	1:4:0.6:4:147	180	5.50	CHA	350	0.51	0.46	0.03	0.49
180_4_5	1:4:0.6:4:147	180	7.00	CHA	368	0.51	0.45	0.04	0.49
180_2_MW	1:2:0.6:2:75	180	7.25	CHA	206	0.50	0.41	0.09	0.50

[a] Particle diameters are given as *Z*-average values of the corresponding Cumulants algorithm.[42,43]

ments (Quantachrome Autosorb MP) at 87 K. Prior to the adsorption experiments, the samples were calcined in air at 550 °C for 24 h (heating rate: 1 °C min^{-1}) and outgassed under vacuum at 350 °C overnight.

Results and Discussion

Synthesis. To obtain colloidal precursor solutions for the synthesis of nanosized silicoaluminophosphates, the same strategy previously employed in $AlPO_n$-18 (AEI structure type code) syntheses was used. First, the molecular or colloidal sources for aluminum and silicon are dissolved in basic media in the presence of tetraethylammonium hydroxide as solvent. The lower threshold in order to obtain a clear solution was a ratio of Al_2O_3:TEA_2O = 1:2 (based on a 35 wt % TEAOH solution). Afterward, the same molar amount of phosphorus is added as concentrated phosphoric acid in order to maintain the solution as concentrated as possible and to neutralize the synthesis solution, as the SAPO-34 phase crystallizes most preferentially under slightly acidic or neutral conditions.[39] According to La Mer and Dinegar,[40] the synthesis of nanocrystals is favored by a high degree of supersaturation at the end of the induction period, which leads to fast and homogeneous nucleation of a high number of nuclei with ideally monomodal size distribution. In a conventional gel system, heterogeneous nucleation most preferentially takes place, and this results in the formation of particles with broad size distributions. Therefore, the ideal precursor solution should be as concentrated as possible but still colloidal to guarantee a real solution with a high degree of supersaturation during the induction heating period. The concentration of the precursor systems was varied, and the temperature of the HT treatment was changed gradually in order to optimize the nucleation and crystallization process. A highly dilute system with an Al_2O_3:TEA_2O:H_2O ratio of 1:4:147 was the starting point. This system guaranteed clear solutions during the whole synthesis procedure; the corresponding precursor solutions did not show a Tyndall effect. Afterward the concentration is increased stepwise to Al_2O_3:TEA_2O:H_2O = 1:2:75, which was the upper limit for the preparation of colloidal precursor solutions. The system was also very sensitive to parameters like room temperature aging (typically ~30 min), speed (450 rpm), and time of stirring during initial dissolution (~2 h), addition rate of H_3PO_4

(39) Prakash, A. M.; Unnikrishnan, S. *J. Chem. Soc., Faraday Trans.* **1994**, *90*, 2291.
(40) La Mer, V. K.; Dinegar, R. H. *J. Am. Chem. Soc.* **1950**, *72*, 4847.

(~0.2 mL min^{-1}), and so forth (these parameters were not systematically investigated and presented in the paper).

All precursor systems were subjected to HT treatment with varying times of crystallization. The heating rate in the used setup is typically ~2.5° min^{-1} (from reference experiments), and quenching to RT was performed under flowing cold water for about 10 min. The samples quenched after short heating time (see Table 1) yielded no solid material after centrifugation or flocculation in low-density solvents like methanol or ethanol. Instead, the systems represented perfectly clear solutions showing no Tyndall effect. This was also the case for the highly concentrated systems showing Tyndall effects before HT treatment. By adding diluted NaCl solution, flocculation is observed, subsequent centrifugation was possible, and some of the resulting products were further subjected to characterization. It is observed that the induction time increased from <2 to <4.5 h for the experiments at 180 °C with decreasing the concentration of Al, P, and Si. In the more diluted systems, the diffusion pathways for the reactive components are increased, which results in slower reaction kinetics.

At 160 °C, AEI was detected in various amounts as a competing phase in the final crystalline products according to XRD. The intergrowth of CHA/AEI phases is reporting extensively in the ExxonMobil patent.[35,37] However, from our XRD and SEM data, the phases appear to be largely separated. AEI forms sheet-like hexagonal crystals, whereas CHA is obtained in the form of cubic crystals. The SAPO-18 phase (AEI-type structure) is structurally related to the chabazite structure.[41] Both include sheets of connected double six-membered rings (D6R). The sheets are connected along the *z*-axis (via O-bridges) to form stacked sheets. The lateral shift between the sheets is zero for the CHA structure, whereas a rotation of 180° about the *z*-axis gives the AEI structure. The connection gives rise to a three-dimensional channel system with eight-membered pore openings of 3.8 Å diameter. This close relationship gives rise to similar energies for both microporous materials; thus, both AEI and CHA-type materials can nucleate at 160 °C in the investigated systems. Additionally, recrystallization from AEI to CHA was observed in the reacting systems with increasing the time of heating (see samples 160_3 and 160_4). The rate of recrystallization is dependent on the initial composition and temperature; however, the recrystallization in the opposite direction is not observed (from CHA to AEI). The experiments performed at 160 °C do not show a steady trend in nucleation times, and this is attributed to the occurrence of two different phases in the final products.

The sizes of the particles after HT treatment increased with synthesis time for all investigated samples. Comparing the different concentrations in the precursor solutions, no clear trend can be seen (Table 1). This is expected, as there are several contributing processes. The smallest primary particles nucleate from the most concentrated precursor solutions. However, after the nucleation, growth of primary particles takes place and the growth rate is faster in more concentrated systems. Additionally, the growth phase is longer when the system is more concentrated or the amount of nuclei is lower (which is the case for less concentrated precursor solutions). Therefore, the size of the resulting particles depends on the elapsed time between nucleation and quenching during the HT treatment. In case of sample 180_2/1_3, the quenching obviously was very shortly after nucleation and the particles showed an average size of 180 nm. However, the yield at that time was very low (~10% of final yield). Between 1.5 and 2.0 h a large increase in size (>50%) was observed for this sample and the growth phase was completed, as no further increase in size was observed after 2.5 h. Similarly, sample 180_2_3 was assumably quenched relatively late, and a fast growth process had already taken place. The resultant size (285 nm) is identical to the system 180_2/1 after the same synthesis time (2 h). In order to synthesize particles of small size, it is therefore necessary to balance the size of primary particles and the proceeding growth rate by careful adjustment of synthesis conditions. In the system 180_3 (lower concentration) this balance is obviously better. After 3 h of aging, the particles are nucleated and grown to a ZD-average size of 264 nm and further growth was very slow (180_3_3–180_3_5). Therefore the final crystals were smaller in diameter than the 180_2 series of samples. The crystalline yields from the investigated syntheses systems were similar. Typically, yields of ~60% were found relatively short after nucleation, and for long synthesis times (>6 h) the yields increased to ~75%. A third contributing process, which is affecting the size of the products, can be deduced from the 180_3 series but also was observed for all systems (not shown). If the synthesis time is further prolonged, particles with sizes of up to ~1 μm are obtained although the yield and degree of crystallinity do not increase. Most probably these large particles result from aggregation of primary particles as the zeta potential is very low (see DLS and ζ-potential section). However, Ostwald ripening cannot be ruled out.

The pH of the synthesis solution was monitored prior to and after HT treatment. The precursor solution showed neutral pH, and due to the relatively high dilution, the pH rose to 7.1, 7.5, and 8.5 with increasing the concentration after the complete condensation process.

All crystalline samples were subjected to elemental analysis after freeze-drying to gain information about the degree of silicon incorporation. The relative molar fractions of the T-elements are shown in Table 1. With increasing the synthesis time, the silicon content increased, but none of the investigated samples reached the Si:Al ratio in the precursor solution of 0.3. A similar result was found earlier by Ashtekar et al.[22] Those samples, which were hydrothermally treated for relatively long times (>6 h) reach a Si molar fraction of 0.08, which corresponds to a composition of $Al_6P_5SiO_{24}\cdot x TEA^+\cdot n H_2O$ (or one silicon atom per chabazite cage containing 12 T-atoms). Obviously, only P-positions of the hypothetical CHA framework are substituted by Si atoms. Tan et al.[24] showed by means of MAS NMR data that a large part (~80%) of the final silicon fraction is incorporated during nucleation in the gel systems and later

(41) Baerlocher, C.; McCusker, L. B. Database of Zeolite Structures. http://www.iza-structure.org/databases/.
(42) Frisken, B. J. *Appl. Opt.* **2001**, *40*, 4087.
(43) Koppel, D. E. *J. Chem. Phys.* **1972**, *57*, 4814.

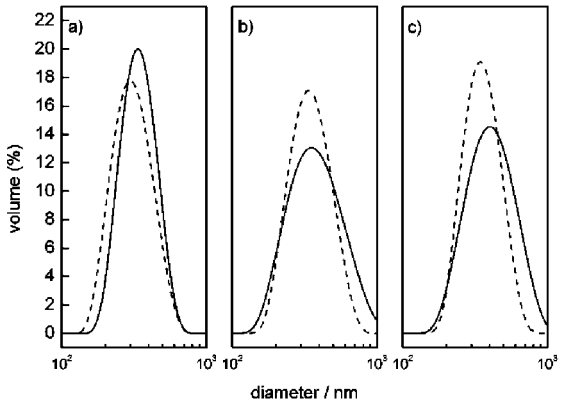

Figure 1. DLS curves of samples 180_4_3–180_4_5 (a–c) after hydrothermal treatment (solid) and after three purification cycles in aqueous KOH solution (dashed). The data are expressed as volume-weighted Contin distribution.

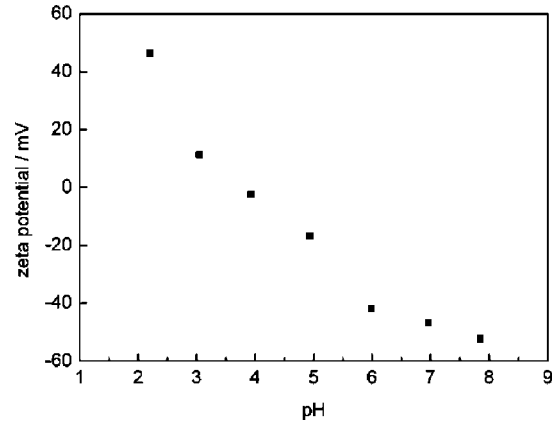

Figure 2. pH dependence of zeta potential value for sample 180_4_5 (the samples were equilibrated in Hydrion buffer solutions and checked for pH with a gel electrode prior the measurements).

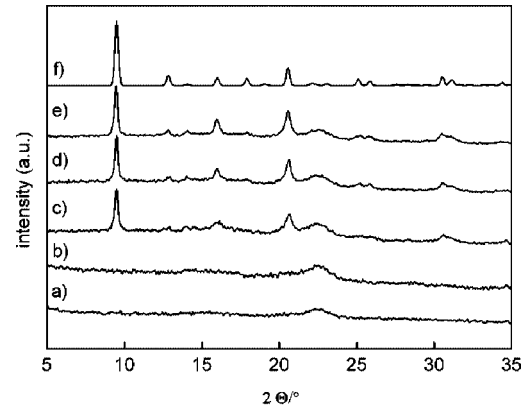

Figure 3. Powder X-ray diffraction patterns of samples 180_4_1–180_4_5 (a−e) and simulated SAPO-34 XRD data (f).[20] The broad peak at ∼22.5° is due to the sample support (filter paper) in the used measuring setup.

substitution of phosphorus atoms only takes place to a minor extent. In our clear precursor systems the situation is slightly different. The products quenched shortly after nucleation show approximately 40% of the final Si substitution, and the remaining Si is incorporated during the crystal growth. However, the fraction of silicon by weight in the total mass of the analyzed products is relatively low (∼1%) resulting in a rather large uncertainty in the shown elemental ratios. This can account for the unexpected values for the samples 160_2_4 and 180_2_4.

DLS and ζ-Potential. DLS data of the series 180_4 are shown in Figure 1. The same sample series has been depicted in the following graphs (the results for all investigated samples were similar). All products showed monodisperse particle size distributions after HT treatment with polydispersity indexes of below 0.1 (This parameter is calculated from the Cumulants analysis[42,43] of the DLS correlation function. If one assumed a single size population following a Gaussian distribution, then the polydispersity index would be related to the standard deviation (σ) and the average mean size (Z_D) of the hypothetical Gaussian distribution: PDI = σ^2/Z_D^2). However, if the samples were washed in double distilled water, they showed varying degrees of polydispersity due to agglomeration. The stability of the suspensions was investigated by the pH-dependent zeta potential measurements of particles stabilized in water (Figure 2). The isoelectric point of the SAPO-34 particles is at pH ∼ 4 due to the acidity of the molecular sieve which is dependent on the degree and distribution of silicon in the CHA framework structure. Consequently, suspensions of SAPO-34 react acidic. The zeta potential reaches values of < −40 mV when the suspensions have pH values above 6. Therefore, we chose slightly basic (pH = 8) aqueous KOH solution for the washing cycles after the complete crystallization of the SAPO-34 samples. Hence, the washed suspensions showed the same or even narrower monomodal size distributions than after HT treatment (Figure 1). At pH > 9 the synthesized samples started to decompose and therefore showed irreproducible zeta potential values.

XRD and SEM Investigations. Figure 3 shows X-ray diffraction patterns of the samples 180_4. The flocculated samples 1 and 2 appear X-ray amorphous after purification and drying. Consequently, SEM images of the freeze-dried samples (Figure 4a,b) show agglomerated particles with undefined morphology. At higher magnification (50000×, not shown) the size of the individual flocculated gel particles can be estimated to be about 100 nm. The samples 3–5 represent crystalline materials with the typical SAPO-34 (CHA) pattern. No phase impurities were detected in this series and in the other experiments conducted at 180 °C, whereas samples treated at 160 °C contain SAPO-18 impurities (AEI). Under increased crystallization time, the particles become bigger in size (Figure 4c−e). Additionally, the morphology of the crystals is better defined, and a flattened cube-like habit is dominant for the particles. Especially the SEM images of sample 180_4_3 show a relatively large amount of material with undefined morphology.

Vibration Spectroscopy. In Figure 5 the Raman spectra of the sample series 180_4 and of aqueous TEAOH are shown. The assignments of Raman and IR bands were based on relevant reports,[22,24,39,44–48] and the data are summarized

(44) Dutta, P. K.; Rao, K. M.; Park, J. Y. *J. Phys. Chem.* **1991**, *95*, 6654.
(45) Marchese, L.; Frache, A.; Gianotti, E.; Martra, G.; Causa, M.; Coluccia, S. *Microporous Mesoporous Mater.* **1999**, *30*, 145.
(46) Pechar, F.; Rykl, D. *Zeolites* **1983**, *3*, 329.
(47) Schnabel, K.-H.; Finger, G.; Kornatowski, J.; Loeffler, E.; Peuker, C.; Pilz, W. *Microporous Mater.* **1997**, *11*, 293.

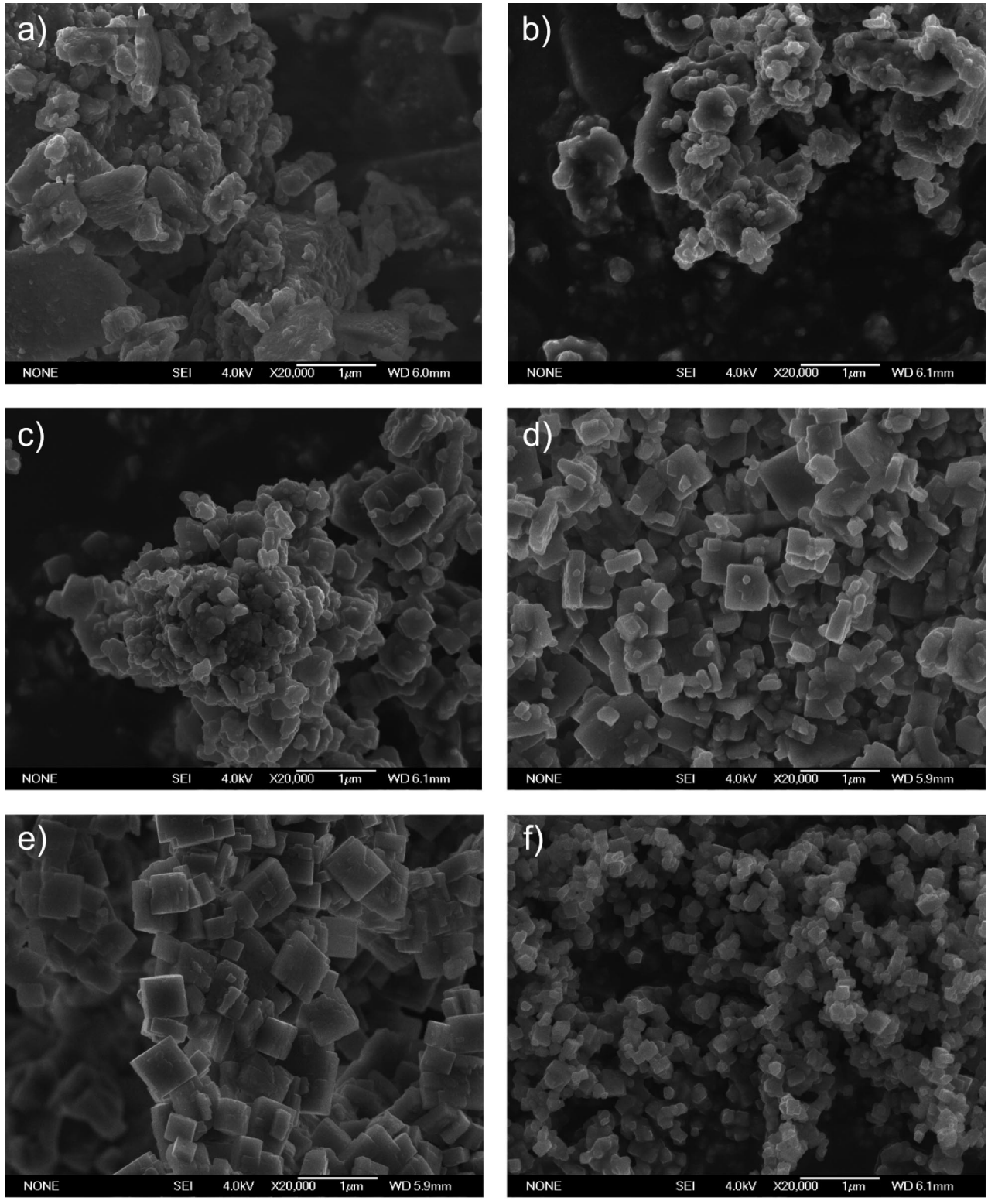

Figure 4. SEM images of samples 180_4_1–180_4_5 (a–e) and 180_2_MW (f).

in Table 2. All bands of the template are present in the solid products indicating that TEA^+ ions interact with the silicoaluminophosphate network at all stages of the crystallization process. However, the samples 1 and 2 represent X-ray amorphous coagulated condensation products, and the template is likely to be captured inside of the gel, rather than incorporated in the framework structure. Tan et al.[24] observed a gradually increasing amount of included template in the silicoaluminophosphates with increasing the synthesis time of the gel systems. The crystalline samples 3–5 showed two structure sensitive bands at 251 and 473 cm^{-1}. The latter

(48) Socrates, G. *Infrared and Raman Characteristic Group Frequencies*; John Wiley & Sons Ltd: Chichester, 2001.

(49) Knops-Gerrits, P.-P.; De Vos, D. E.; Feijen, E. J. P.; Jacobs, P. A. *Microporous Mater.* **1997**, *8*, 3.

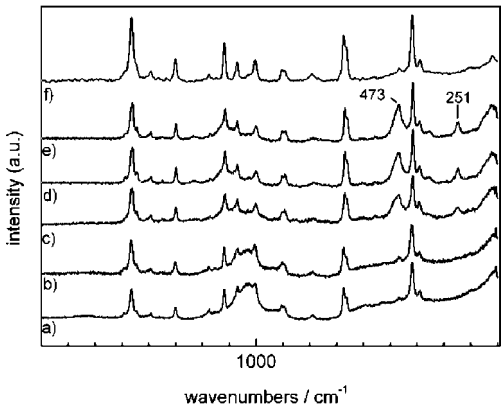

Figure 5. Raman spectra of samples 180_4_1–180_4_5 (a–e) and of aqueous tetraethyl ammonium hydroxide solution (f).

Table 2. Assignments of Vibrational Bands in the SAPO-34 Material[22,24,39,44–48]

IR bands (wavenumbers/cm^{-1})	Raman bands (wavenumbers/cm^{-1})	assignment
1213		ν_A P−O−Al
1122		ν_A O−P−O
1005		ν P−O
644		δ T−O (D6R)
571		δ T−O (PO4)
532		δ T−O (Si/AlO4)
488		δ T−O (SiO4)
	473	ν_S T−O−T
390		δ T−O
	251	ν T−N

can be assigned to the symmetric T−O−T stretching vibration,[49] whereas the first vibration is attributed to a T−N stretching.[45] IR spectra (Figure 6) of the same samples are dominated by a broad band at ∼1100 cm^{-1} assigned to an O−P−O asymmetric stretching vibration. As expected, this band is present in both amorphous and crystalline samples but shifted to 1120 cm^{-1} in the crystalline samples. The two X-ray amorphous samples differ from each other by the appearance of a P−O−Al asymmetric stretching band (1213 cm^{-1}) and a P−O (1005 cm^{-1}) stretching band, which only appear after the formation of a certain fraction of crystalline units in the synthesis suspensions. Consequently, these bands are also found in the crystalline samples. Characteristic framework vibration bands are seen in the crystalline SAPO-34 samples in the T−O bending region at 644, 571, 532,

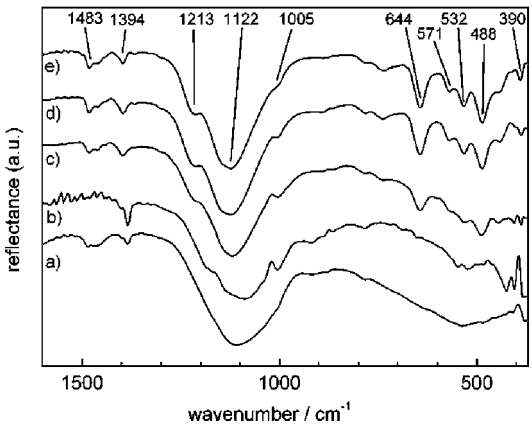

Figure 6. Diffuse reflectance infrared Fourier spectroscopy (DRIFT) data for samples 180_4_1–180_4_5 (a–e).

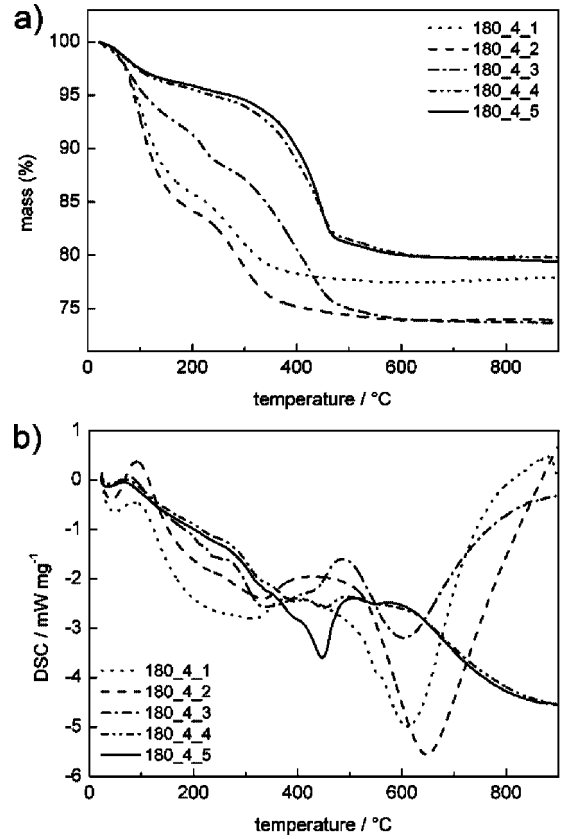

Figure 7. Thermogravimetric (a) and differential scanning calorimetric (b) data of samples 180_4_1–180_4_5.

and 488 cm^{-1}. The band at 390 cm^{-1} was found in all investigated samples.

TGA and DSC Data. In Figure 7 TGA and DSC data of the samples 180_4_1–5 are shown. The samples 4 and 5 show nearly identical TGA behavior. These samples lose ∼4% of water upon heating to 100 °C and a small endothermic peak is observed in the DSC curve. The exothermic decomposition of the template molecules proceeds in two steps at 400 °C (14%) and 520 °C (2%). These weight losses correspond to two H_2O molecules and one TEA^+ molecule per chabazite cage (the TEA^+ molecule is expected for the charge compensation of one Si atom, cp. elemental analysis). The water loss in the samples 1–3 is much larger (14, 16, and 8%, respectively) due to a higher fraction of noncondensed hydroxyl groups, which is expected for the amorphous samples (1 and 2). Obviously, a reasonable fraction of sample 180_4_3 is not in a fully condensed state. The amorphous samples lose 12 and 9% of their weight upon further heating to 240 °C. This weight loss is attributed to the decomposition of weakly connected template with the inorganic matrix. Sample 3 also loses 4% at this temperature, but a larger fraction (14%) of template is removed at higher temperature, indicating a stronger interaction of the template within the crystalline framework structure. Interestingly, the samples 1–3 show large exothermic DSC signals at ∼600 °C, which is due to a phase transformation to the tridymite phase (proved by XRD).

Microwave Synthesis. One of the major goals in the synthesis of nanosized molecular sieves is to render the synthesis mixture as homogeneous as possible in terms of

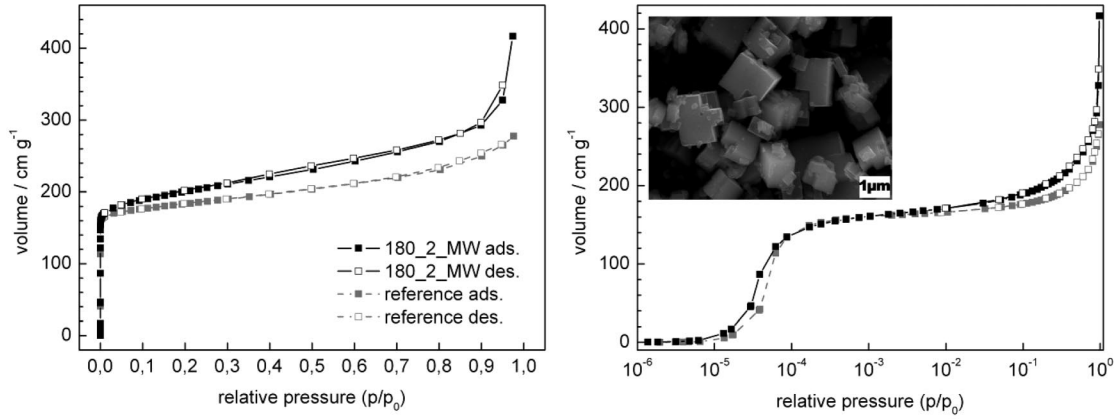

Figure 8. Argon physisorption isotherms of sample 180_2_MW (black) and a micrometer-sized reference sample (grey). Left, linear scale; right, logarithmic scale. Inset: SEM image of the reference sample with magnification of 15000.

composition and temperature. Additionally, for the investigated systems a very fast heating rate can avoid the formation of AEI impurities. These parameters can only be controlled to a limited degree in conventional autoclaves and ovens. Therefore we used microwave (MW) energy for heating of different precursor systems. The most successful experiment performed in the MW oven abbreviated as 180_2_MW is listed in Table 1. The precursor solution of molar composition 1 Al_2O_3:2 P_2O_5:0.6 SiO_2:2 TEA_2O:75 H_2O was treated at 180 °C (heating rate of 32 °C min^{-1} for a duration of 7.25 h). The obtained particles had an average particle diameter of 200 nm (PDI = 0.090), and no AEI impurities were detected in the XRD pattern (not shown). This particle diameter is exceptionally small for (silico)aluminophosphate systems.[1] SEM images (Figure 4f) show particles with a homogeneous cube-like morphology. Besides, a large fraction of the powder consists of particles with diameters around 100 nm.

Sorption Properties. To evaluate the effect of crystal size on the sorption properties of the nanosized crystals, a reference material according to the original work by Lok et al. (Example 35) was prepared.[18] The resulting sample synthesized from a conventional gel was highly crystalline and has particle sizes above 1 μm. Figure 8 shows the argon physisorption isotherms of sample 180_2_MW in comparison with the reference sample. In this case, argon was used as the probe molecule (diameter: 3.42 Å[50]) as the CHA structure has pore openings of 3.8 Å. The graphs (logarithmic scale, right image in Figure 8) show that the micropores of both materials are starting to be filled at a relative pressure of 1×10^{-5} and the process is completed at 1×10^{-4} p/p_0. This exceptionally steep loading curve is typical for CHA and AEI (silico)aluminophosphates (also for other adsorptive, e.g., water). As it is expected, the nano- and micrometer-sized samples show the same micropore volume, as both are fully crystalline. At higher relative pressure, adsorption in the interparticle voids of the material takes place (left image). The degree of textural porosity is much larger in the nanosized samples, and another 125 cm^3 g^{-1} (43% of total adsorbed amount of argon, 34% for the reference sample) is adsorbed.

Conclusions

By the use of colloidal precursor solutions we were able to synthesize SAPO-34 particles with diameters smaller than 300 nm. By means of microwave hydrothermal treatment the diameter was further reduced to 100 nm, and the resultant material was fully crystalline with a well-defined cube-like morphology. All investigated products showed narrow particle distributions, and the resultant suspensions were electrostatically stabilized in basic media. In the precursor solutions, tetraethylammonium hydroxide is used as the structure-directing agent and the final chemical composition was varied in the following range: 1 Al_2O_3:2–4 P_2O_5:0.6–1 SiO_2:2–4 TEA_2O:75–147 H_2O. The kinetic study is consistent with a mechanism of crystallization: upon heating of the clear precursor mixtures the dissolved Al-, P-, and Si- sources start to react and form precursor species until a certain degree of supersaturation, which is dependent on composition and temperature of heating. Then, nucleation of primary particles takes place within the amorphous species and the particles condense and form crystalline aggregates. Simultaneously, these particles grow by further addition of nutrients from the synthesis solution until they reach their final size. Additionally, at a relatively later stage of heating, aggregation and condensation of secondary particles or Ostwald ripening take place.

Acknowledgment. This work is part of the joint network "New highly porous materials and systems for energy storage and heat transformation" financed by the German Ministry of Education and Research (BMBF), FKZ01SF0303.

CM703541W

(50) Krishna, R.; van Baten, J. M. *Microporous Mesoporous Mater.* **2008**, *109*, 91.